Programming Semiconductor Nanowire

Composition with Sub-100-nm Resolution via the

Geode Process

Maritza Mujica^a, Amar Mohabir^a, Pralav P. Shetty^b, Wesley R. Cline^a, Daniel Aziz^a, Matthew T. McDowell^{b,c}, Victor Breedveld^a, Sven Holger Behrens^d and Michael A. Filler^a*

a School of Chemical & Biomolecular Engineering, Georgia Institute of Technology, Atlanta, Georgia, 30332, United States

^b George W. Woodruff School of Mechanical Engineering, Georgia Institute of Technology,

Atlanta, Georgia, 30332, United States

^c School of Materials Science and Engineering, Georgia Institute of Technology, Atlanta,
Georgia, 30332, United States

^d Polymer Science and Materials Chemistry, Exponent, Inc., 3350 Peachtree Road NE, Suite 1125, Atlanta, Georgia 30326, United States

KEYWORDS

Nanowires, Silicon, Germanium, Vapor-liquid-solid, Nanomanufacturing

ABSTRACT

We demonstrate the vapor-liquid-solid growth of single-crystalline i-Si, i-Si/n-Si, and Si_xGe_{1-x}/Si_yGe_{1-y} nanowires via the Geode Process. By enabling nanowire growth on the large internal surface area of a microcapsule powder, the Geode Process improves the scalability of semiconductor nanowire manufacturing while maintaining nanoscale programmability. Here, we show that heat and mass transport limitations introduced by the microcapsule wall are negligible, enabling the same degree of compositional control for nanowires grown inside microcapsules and on conventional flat substrates. Efficient heat and mass transport also minimize the structural variations of nanowires grown in microcapsules with different diameters and wall thicknesses. Nanowires containing at least 16 segments and segment lengths below 75 nm are demonstrated.

TEXT

Introduction

There remains a need for semiconductor nanowire manufacturing processes that simultaneously offer scalability and nanoscale control of composition. Semiconductor nanowires are promising building blocks for future electronic, ¹⁻⁵ photonic, ^{6, 7} energy, ^{8, 9} and biological ¹⁰⁻¹² applications. The vapor-liquid-solid (VLS) mechanism is a workhorse tool in this regard, permitting the growth of nanowire heterostructures such as Si/SiGe, ^{1, 13-15} InAs/InP, ¹⁶ and GaS/GaP⁶ as well as superlattices of Si/SiGe¹⁷ and InAs/InP^{18, 19} by switching between precursors during growth. At the same time, most VLS growth occurs on flat substrates. While useful in many situations (e.g., device integration²⁰), the ultimate cost and throughput of nanowires grown on flat substrates will be limited by the constraints of 2-D scaling. Many existing and future applications will require large quantities of compositionally controlled semiconductor nanowires and devices.

Existing techniques, such as Aerotaxy²¹⁻²³ and solution-liquid-solid (SLS) growth,²⁴⁻²⁷ offer scalability or robust nanoscale compositional control but generally not both. Nanowires with two axial segments, each with a length of \sim 1 μ m, have been shown with Aerotaxy.²³ However, the short reactor residence of times (\sim 1 sec) complicate the growth of nanowires with significantly more or shorter segments. SLS growth permits nanowires with segment lengths below 20 nm,²⁵ but morphology and uniformity are inferior to that of compositionally homogeneous nanowires.²⁶, ²⁷ SLS growth in a microfluidic reactor permits nanowires with \sim 8 segments and segment lengths as small as 100 nm,²⁴ but this approach limits scalability.

The Geode Process²⁸ offers a route to increase manufacturing throughput by leveraging the high surface area of silica microcapsule powders while also maintaining the ability to program

nanowire composition via the VLS mechanism. Silica microcapsules exhibit porous walls to facilitate gaseous precursor transport and are lined on their interior with the metal nanoparticles that catalyze VLS growth. Bulk microcapsule powders are synthesized in a scalable process that includes emulsion-templating to form the microcapsule, sedimentation to improve microcapsule uniformity, and finally drying and calcination to create a flowable powder. "Microgeode" powders are formed upon VLS growth of semiconductor nanowires on the microcapsule interiors. To date, the synthesis of microcapsule and Si nanowire microgeode powders have been demonstrated.²⁸

Synthesizing nanowires with precise structural and compositional encoding via the Geode Process depends on the rate of heat and mass transport through the microcapsule wall. Mass transport is governed by microcapsule wall thickness and porosity while heat transport is governed by the thermal conductance of the microcapsule wall, which depends on its composition (i.e., silica) as well as thickness and porosity. At high transport rates, precursor pressure and temperature on the microcapsule interior would be equivalent to that for flat substrates. Since precursor pressure and growth temperature play a critical role in nanowire growth via the VLS mechanism,²⁹
³⁴ moderate to low transport rates would likely result in nanowires with different structures and compositions inside microcapsules relative to those on flat substrates or perhaps no growth at all.³⁵.

³⁶ Moreover, in cases where transport limitations are non-negligible, powders with a distribution of microcapsule structures (e.g., capsule diameter, wall thickness) would likely result in a distribution of nanowire structures (e.g., segment lengths, tapering, doping) and necessitate the inclusion of purification steps to compensate.

Here, we study the VLS growth of three types of semiconductor nanowires inside hollow microcapsules: nominally intrinsic Si (i-Si), phosphorus-modulated Si (i-Si/n-Si), and heterostructured SiGe alloy $(Si_xGe_{1-x}/Si_yGe_{1-y})$ nanowires. We find that as-synthesized

microgeodes contain dense networks of single-crystalline nanowires, thus permitting the use of conventional Raman spectroscopy to assess their crystallinity. The achievable compositional programming of Si_xGe_{1-x}/Si_yGe_{1-y} nanowires inside hollow microcapsules is essentially indistinguishable from that on flat substrates. For Si_xGe_{1-x}/Si_yGe_{1-y} nanowires, we show the programming of at least 16 segments, segment lengths below 75 nm, and nanowire-to-nanowire segment length variations of less than 6%. These data confirm efficient heat and mass transport through the microcapsule wall, underscoring the promise of the Geode Process for the scalable synthesis of semiconductor nanowires with programmable compositions.

Results and Discussion

Silica microcapsule powders suitable for the Geode Process are synthesized via emulsion templating, sedimentation separation, freeze-drying, and calcination (Supporting Information, Methods). Figure 1 shows as-synthesized microcapsules at multiple length scales. Microcapsule powders appear white and are flowable (Figure 1a). Scanning electron microscopy (SEM) shows that microcapsules are spherical and enclosed (Figures 1b and 1c). The average microcapsule diameter is $12 \pm 7 \, \mu m$ and the average microcapsule wall thickness is $1.2 \pm 0.4 \, \mu m$. The Au nanoparticles that catalyze VLS growth line the microcapsule inner surface (Figure 1d, top) but not the outer surface (Figure 1d, bottom). Otherwise, the morphology of the microcapsule wall appears similar on the inner and outer surfaces.

Microcapsule powders serve as a high surface area substrate for semiconductor nanowire growth. A custom-fabricated microcapsule powder holder is used during nanowire growth to prevent contamination of the chemical vapor deposition reactor (Supporting Information, Figure

S1). Figure 2 shows SEM images of microgeodes intentionally opened with mild sonication following the growth of i-Si (Figures 2a and 2b) and i-Si/n-Si nanowires (Figures 2c and 2d). In both cases, microgeodes exhibit dense internal nanowire growth and limited external growth, along with nanowire morphologies consistent with growth on flat substrates. Note the uniformity of microcapsule wall thickness in both cases. The SEM image in Figure 2e, which follows selective i-Si segment etching with KOH, confirms the compositional encoding of i-Si/n-Si nanowires inside microgeodes.³⁷

We use conventional, diffraction-limited Raman spectroscopy to analyze nanowire crystallinity, which highlights the ability of the Geode Process to generate large quantities of material. Nanowires grown on flat substrates tend not to offer sufficient signal-to-noise ratio for a similar measurement. Raman spectra of empty microcapsules (i.e., prior to nanowire growth) show no Raman peaks (Figure 2f, bottom), as anticipated for amorphous silica nanoparticles. Spectra for i-Si (Figure 2f, middle) and i-Si/n-Si (Figure 2f, top) nanowire ensembles inside intentionally opened microgeodes show intense peaks near 508 and 510 cm⁻¹, respectively. These peaks result from the longitudinal optical (LO) phonon of c-Si,^{38, 39} which supports the single-crystallinity of Si nanowires inside microgeodes. The 10-12 cm⁻¹ redshift relative to that for bulk c-Si is consistent with that for Si nanowires with Raman laser-induced heating, as would be expected due to the low thermal conductivities of the surrounding air and partial silica microcapsule shell.⁴⁰

Si_xGe_{1-x}/Si_yGe_{1-y} nanowires serve as a model system to demonstrate the compositional programming that can be achieved inside microgeodes. Figure 3 shows two methods for characterizing axial composition: selective etching of Ge-rich segments in H₂O₂ solution and energy dispersive spectroscopy (EDS). To visualize segment etching, we use an intentionally lower density of Si_xGe_{1-x}/Si_yGe_{1-y} nanowires containing segments of alternating composition and

lengths (Figures 3a and 3b). Microgeodes with larger densities of Si_xGe_{1-x}/Si_yGe_{1-y} nanowires are readily possible (Supporting Information, Figure S2), but dense growth makes it difficult to interrogate the wire structures in detail. The majority of nanowires exhibit alternating etched (Gerich) and unetched (Si-rich) segments with lengths of ~350 and ~670 nm, respectively. The Aurich seed nanoparticles that catalyze VLS growth are visible as bright spots at the tip of some nanowires. We observe at least 16 distinct axial segments in individual nanowires (Supporting Information, Figure S3). Unetched Si_xGe_{1-x}/Si_yGe_{1-y} nanowires harvested from microgeodes following sonication show a periodic sequence of darker and brighter regions (Figure 3c), which correspond to the Si-rich and Ge-rich segments.⁴¹ After selective etching (Figure 3d), these harvested Si_xGe_{1-x}/Si_yGe_{1-y} nanowires exhibit the same morphology as nanowires still inside microgeodes (Figures 3a and 3b). EDS mapping of the Ge Lα edge from Si_xGe_{1-x}/Si_yGe_{1-y} nanowires inside an intentionally opened microgeode further confirms the ability to encode composition (Figure 3e), and is consistent with the SEM images of etched and unetched nanowires (Figures 3b-d).

Transmission electron microscopy (TEM) and scanning TEM (STEM) provide more detailed insight into $Si_xGe_{1-x}/Si_yGe_{1-y}$ nanowire composition and structure. High angle annular dark field (HAADF) STEM (Figure 3f) reveals Si_xGe_{1-x} and Si_yGe_{1-y} segments consistent with those imaged with SEM (Figure 3c). EDS maps (Figure 3g) of Au (top), Ge (middle), and Si (bottom) also show the expected composition profile. The nanowire seed particle is largely Au (70.4 at.%), but also contains Si (12.8 at.%) and Ge (16.8 at.%). EDS shows that one segment type is Si-rich ($Si_{65}Ge_{35}$) while the other segment type is Ge-rich (Si_4Ge_{96}). Upon transitioning from the Si_6SGe_{35} segment to the Si_6SGe_{35} segment, the interface width is ~20 nm, but it is ~90 nm upon transitioning from the Si_4Ge_{96} segment to the Si_6SGe_{35} segment. Periwal et al. observe a similar

trend for Si/SiGe nanowires grown on flat substrates, which they attribute to the reservoir effect and the difference in Si and Ge solubility in the Au seed particle.^{13, 15} Bright-field TEM shows one transition between Si₄Ge₉₆ and Si₆₅Ge₃₅ as well as the seed particle at the nanowire tip (Figures 3h and 3i). Selected area electron diffraction (Supporting Information, Figure S4) and nanobeam diffraction (Figure 3h and Supporting Information, Figure S5) analysis confirm that the Si₆₅Ge₃₅ and Si₄Ge₉₆ segments are single crystalline and oriented in the same direction.

Changes to Si_xGe_{1-x} and Si_yGe_{1-y} segment growth time allow for control over segment length but do not appreciably change nanowire morphology, segment composition, or crystal structure. Figure 4 shows data analogous to Figure 3 but for $Si_{65}Ge_{35}/Si_4Ge_{96}$ nanowires with variable $Si_{65}Ge_{35}$ segment lengths separated by Si_4Ge_{96} segments of fixed length. Not only do these data confirm the programmability of segment length for nanowires grown inside microcapsules, but they highlight the ability to control segment length with sub-100-nm resolution (72 \pm 4 nm).

A comparison of segment growth rate for $Si_{65}Ge_{35}/Si_4Ge_{96}$ nanowires grown on flat substrates and in microcapsules demonstrates that heat and mass transport limitations are negligible. Figure 5a shows $Si_{65}Ge_{35}$ segment length as a function of $Si_{65}Ge_{35}$ segment growth time for nanowires grown on flat substrates (magenta, open square) and inside microcapsules (magenta, solid square) in the same reactor run. The lengths of the fixed-length Si_4Ge_{96} segments on flat substrates (gray, open triangle) and inside microcapsules (gray, solid triangle) are also shown. $Si_{65}Ge_{35}$ segment length increases linearly with segment growth time for both substrate types; yielding nearly identical growth rates of 13.8 nm/s and 13.7 nm/s for flat substrates and microcapsules, respectively. All segments exhibit variations in length of no more than 6.5% of their average length. Figure 5b directly compares the segment lengths inside microcapsules to those on flat substrates. The data fall near the y = x line, indicating little difference in growth rate

between growth in microcapsules and on planar substrates, and underlining excellent control of the segment lengths. Since the nanowires measured here are harvested from many microgeodes, this analysis also indicates that variations in growth from microcapsule-to-microcapsule are small. These data confirm that the heat and mass transport limitations introduced by the microcapsule wall are minimal, and that the microcapsule internal temperature and precursor partial pressure are nearly identical to those on the outside.

The rate of precursor transport relative to nanowire growth can be more quantitatively understood using time $\sim \text{length}^2/\text{diffusivity}$. The diffusivity of silane in the microcapsule wall, assuming randomly packed spheres, at the growth conditions is $\sim 10^{-6}$ m²/s. If the microcapsule wall thickness is $\sim 10^{-6}$ m, the timescale for silane to traverse the microcapsule wall is $\sim 10^{-6}$ s. Since the time between nucleation events at the nanowire growth front (i.e., liquid/solid interface) is $\sim 10^{-3}$ s, precursor transport is ~ 3 orders-of-magnitude faster than nanowire growth. Since the process is so strongly limited by nanowire growth rate, even an order-of-magnitude variation in microcapsule wall porosity or thickness is unlikely to significantly impact nanowire structure.

The data in Figure 5b do show subtle differences worthy of mention: Si₆₅Ge₃₅ and Si₄Ge₉₆ segments grown inside microcapsules are slightly longer and shorter, respectively, than those grown on planar substrates. We suspect the high reactivity of GeH₄ at the growth temperature⁴² is responsible for this observation. GeH₄ decomposition on the interior of the microcapsule wall would reduce the internal GeH₄ partial pressure and thus nanowire growth rate, an effect that would be largest for the Si₄Ge₉₆ segments. Additional studies are underway to further clarify these effects, which do not interfere with the control of nanowire heterostructure.

The present study shows the potential of the Geode Process to achieve scalable growth of nanowires with controlled heterostructures, but additional work is needed to advance toward a viable nanomanufacturing technology. In many but not all situations, nanowire harvesting from the microgeode interior and stabilization in dispersion will be necessary. Here, we demonstrate sonication as a preliminary nanowire removal method. Future studies will focus on methods that combine mechanical and chemical approaches as well as surface functionalizations^{43,44} to prevent nanowire agglomeration upon extraction. Fabrication of functional nanowire devices leveraging the programmability demonstrated herein is another logical next step. This work also highlights the need for characterization methods that can statistically assess the distribution of structures and electronic properties^{45,46} of nanowires in bulk samples.

Conclusion

We demonstrate the programmable synthesis of compositionally-modulated semiconductor nanowires inside microcapsule powders via the Geode Process. Three nanowire systems are investigated: i-Si, i-Si/n-Si, and Si_xGe_{1-x}/Si_yGe_{1-y}. Nanowire microgeodes containing dense internal networks of single crystalline nanowires are obtained. Detailed characterization of Si_xGe_{1-x}/Si_yGe_{1-y} nanowires shows that heat and mass transport limitations due to the microcapsule wall are negligible. This feature enables nanowire composition to be controlled with a precision like that on conventional flat substrates and reduces microcapsule-to-microcapsule variability even for different microcapsule diameters and wall thicknesses. The synthetic capabilities demonstrated here set the stage for scalably fabricating and harvesting functional nanoelectronic devices inside microcapsules.

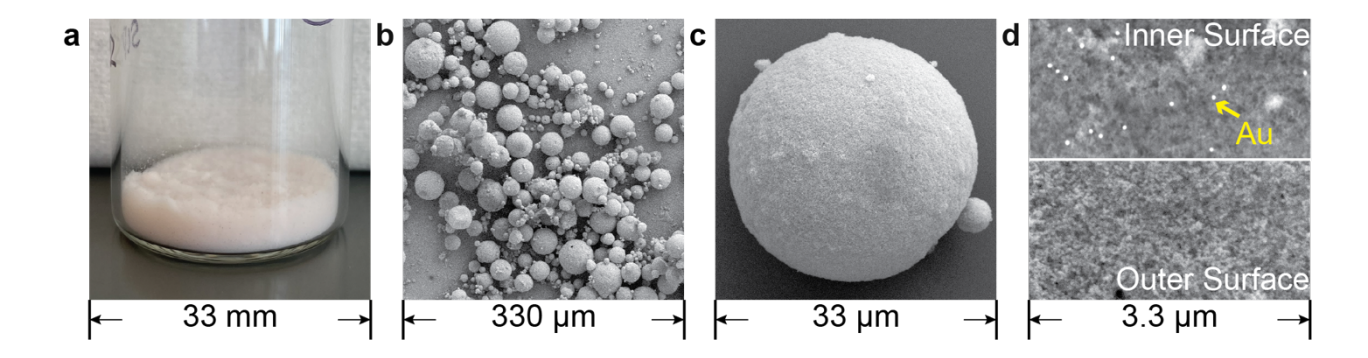


Figure 1. Microcapsule powder. (a) Photograph of bulk microcapsule powder in glass vial. Representative SEM images of (b) microcapsule powder, (c) single microcapsule, (d) inner microcapsule surface with Au catalyst particles (top) and outer microcapsule surface (bottom).

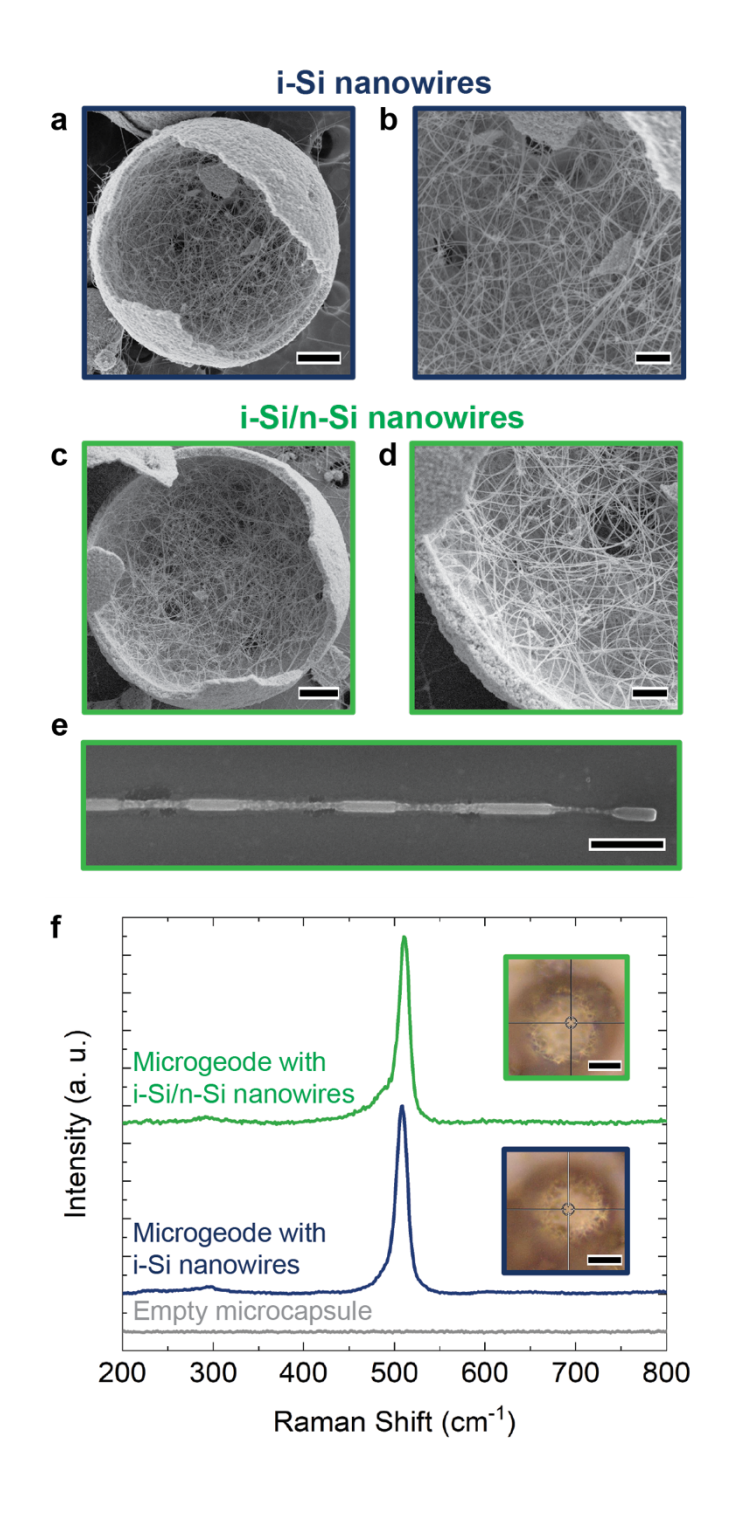


Figure 2. Microgeodes containing i-Si and i-Si/n-Si nanowires. Representative SEM images of intentionally opened microgeodes containing (a-b) i-Si nanowires and (c-d) i-Si/n-Si nanowires. Scale bars: (a, c) 5 μ m; (b, d) 2 μ m. (e) SEM image of a representative i-Si/n-Si nanowire following KOH etching. (f) Raman spectra of empty microcapsules (bottom) as well as intentionally opened

microgeodes containing i-Si (middle) and i-Si/n-Si (top) nanowires. Insets are optical images of the microgeode from the Raman microscope that show the location of spectral data acquisition. Scale bars: $10~\mu m$.

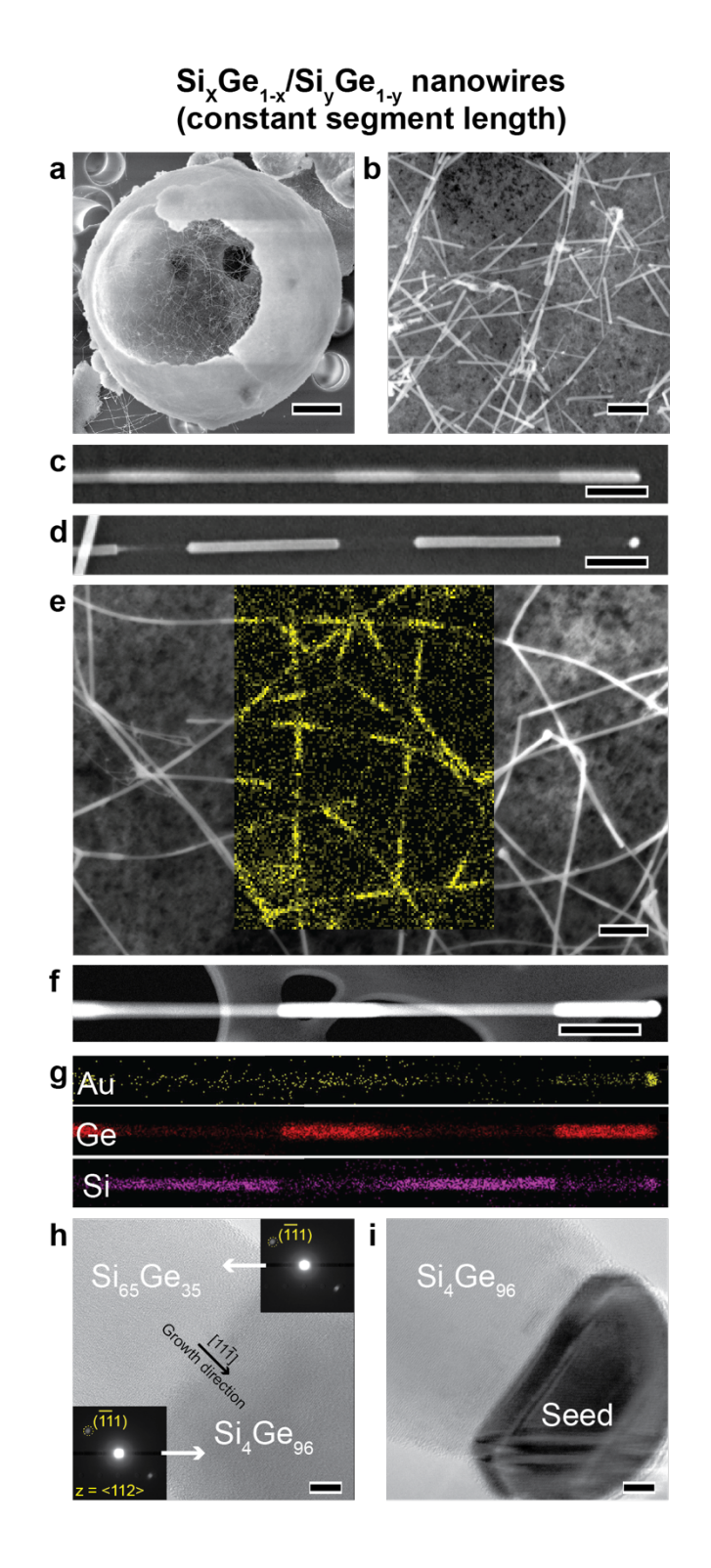


Figure 3. Microgeodes containing $Si_xGe_{1-x}/Si_yGe_{1-y}$ nanowires with constant segment lengths.

Representative SEM images of an intentionally opened microgeode containing $Si_xGe_{1-x}/Si_yGe_{1-y}$ nanowires with constant segment lengths after selective etching at (a) low-magnification and (b)

high-magnification. Scale bars: 5 μm and 500 nm, respectively. SEM images of (c) as-grown and (d) selectively etched nanowires harvested from microgeodes and observed on track-etched membranes. Scale bars: 300 nm. (e) EDS mapping of nanowires inside a microgeode showing Ge Lα EDS map in yellow overlaid onto an SEM image of scanned region. Scale bar: 500 nm. (f) Representative dark-field STEM image of nanowire harvested from a microgeode. Scale bar: 300 nm. (g) Au (top), Ge (middle), and Si (bottom) EDS map of a nanowire harvested from a microgeode. Representative TEM images of nanowire harvested from a microgeode showing (h) Si₄Ge₉₆ and Si₆₅Ge₃₅ segments and (i) region near the nanowire tip. Scale bars: 5 nm. Insets in (h) are nanobeam diffraction patterns of Si₆₅Ge₃₅ and Si₄Ge₉₆ regions along the <112> zone axis and with a [111] nanowire growth direction.

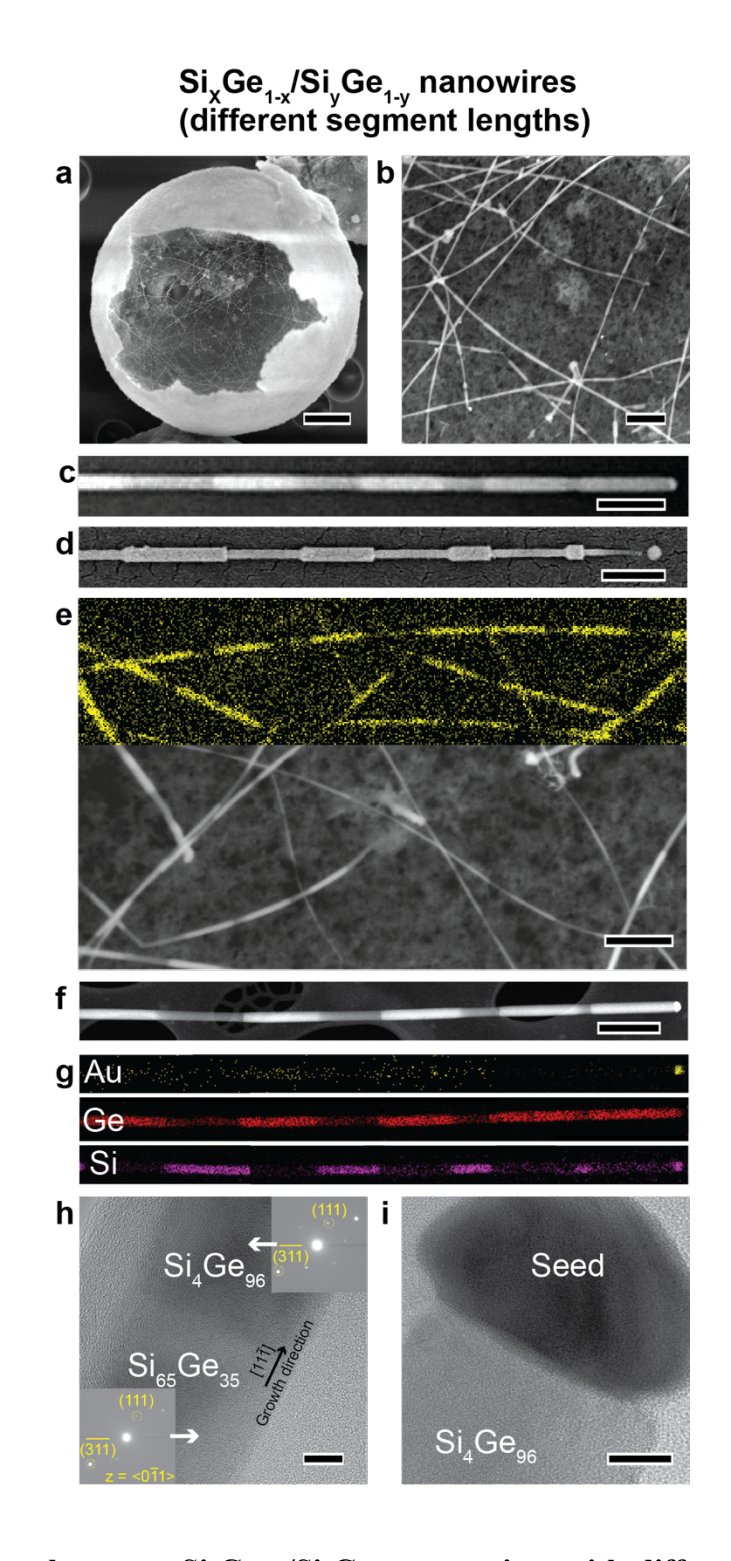


Figure 4. Microcapsule-grown Si_xGe_{1-x}/Si_yGe_{1-y} nanowires with different segment lengths.

SEM images of an intentionally opened microgeode containing $Si_xGe_{1-x}/Si_yGe_{1-y}$ nanowires with different segment lengths after selective etching at (a) low-magnification and (b) high-

magnification. Scale bars: 5 μ m and 500 nm, respectively. SEM images of sonicated out variable Si_xGe_{1-x}/Si_yGe_{1-y} nanowires from nanowire geodes and observed on top of track-etched membranes (c) as-grown and (d) selectively etched. Scale bars: 300 nm. (e) EDS mapping of nanowires inside a microgeode showing Ge L α EDS map in yellow overlaid onto an SEM image of scanned region. Scale bar: 500 nm. (f) Representative dark-field STEM image of nanowire harvested from a microgeode. Scale bar: 300 nm. (g) Au (top), Ge (middle), and Si (bottom) EDS map of a nanowire harvested from a microgeode. Representative TEM images of nanowire harvested from a microgeode showing (h) Si₄Ge₉₆ and Si₆₅Ge₃₅ segments and (i) region near the nanowire tip. Scale bars: 10 nm. Insets in (h) are nanobeam diffraction patterns of Si₆₅Ge₃₅ and Si₄Ge₉₆ regions along the $<0\overline{1}1>$ zone axis and with a [11 $\overline{1}$] nanowire growth direction.

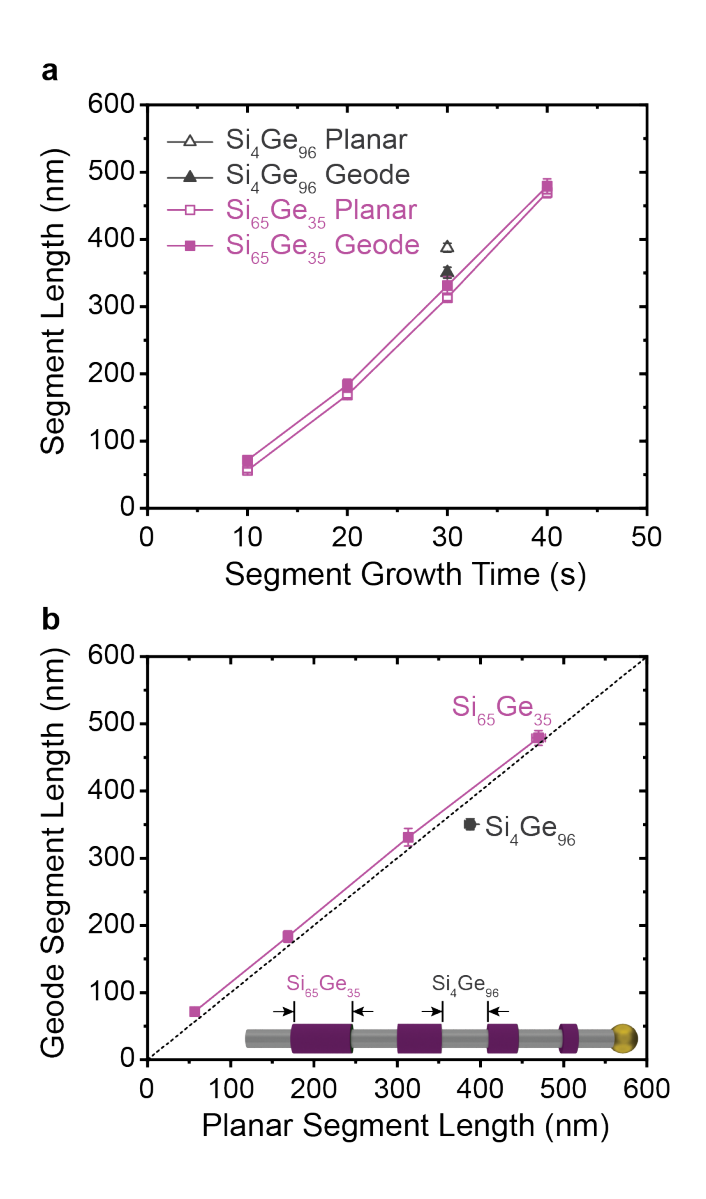


Figure 5. Comparison of nanowire segment growth on planar and microcapsule substrates.

(a) Segment growth rate as a function of growth time for $Si_{65}Ge_{35}$ segments (magenta squares) and Si_4Ge_{96} (gray triangles) for planar (open symbols) and microcapsule (filled symbols) substrates. (b) x-y plot of $Si_{65}Ge_{35}$ and Si_4Ge_{96} segment lengths for nanowires grown on planar substrates and those harvested from microgeodes. The dashed y = x line is included as a guide to the eye. ASSOCIATED CONTENT

Supporting Information

Additional figures showing the custom-built microcapsule powder holder, selective etching of

Si_xGe_{1-x}/Si_yGe_{1-y} nanowires, and diffraction analysis, as referenced in the main text. This

material is available free of charge via the Internet at http://pubs.acs.org.

AUTHOR INFORMATION

Corresponding Authors

*To whom correspondence should be addressed: michael.filler@chbe.gatech.edu

Author Contributions

MAF, SHB, and VB conceived of the Geode process. MM conducted emulsion templating

experiments, microcapsule formation, and microcapsule characterization. ATM and MM

developed nanowire growth. PPS conducted TEM and STEM characterization. WRC and DA

assisted with nanowire harvesting and selective etching. PPS and MTM analyzed the TEM and

STEM data. MM, VB, SHB, and MAF jointly designed the experiments, analyzed the data, and

wrote the manuscript. All authors approved the final version.

Notes

The authors declare no competing financial interest.

Funding Sources

National Science Foundation

ACKNOWLEDGMENT

19

The authors gratefully acknowledge the support of the National Science Foundation under Grant No. CBET-1805015. This material is based upon work supported by the National Science Foundation Graduate Research Fellowship under Grant No. DGE-1650044. Any opinions, findings, and conclusions or recommendations expressed in this material are those of the author(s) and do not necessarily reflect the views of the National Science Foundation. This work was performed in part at the Georgia Tech Institute for Electronics and Nanotechnology, a member of the National Nanotechnology Coordinated Infrastructure (NNCI), which is supported by the National Science Foundation (ECCS-2025462).

ABBREVIATIONS

Au, Gold; Si, Silicon; Ge, Germanium; SEM, scanning electron microscope; EDS, electrondispersive X-ray spectroscopy; STEM, scanning transmission electron microscopy; TEM, transmission electron microscopy

REFERENCES

- 1. Brouzet, V.; Salem, B.; Periwal, P.; Alcotte, R.; Chouchane, F.; Bassani, F.; Baron, T.; Ghibaudo, G., Fabrication and electrical characterization of homo- and hetero-structure Si/SiGe nanowire tunnel field effect transistor grown by vapor–liquid–solid mechanism. *Solid-State Electronics* **2016**, *118*, 26-29.
- 2. Yang, C.; Barrelet, C. J.; Capasso, F.; Lieber, C. M., Single p-Type/Intrinsic/n-Type Silicon Nanowires as Nanoscale Avalanche Photodetectors. *Nano Letters* **2006**, *6* (12), 2929-2934.
- 3. Yang, C.; Zhong, Z.; Lieber, C. M., Encoding Electronic Properties by Synthesis of Axial Modulation-Doped Silicon Nanowires. *Science* **2005**, *310* (5752), 1304.
- 4. Lu, W.; Xiang, J.; Timko, B. P.; Wu, Y.; Lieber, C. M., One-Dimensional Hole Gas in Germanium/Silicon Nanowire Heterostructures. *Proceedings of the National Academy of Sciences of the United States of America* **2005**, *102* (29), 10046-10051.
- 5. Wen, C. Y.; Reuter, M. C.; Bruley, J.; Tersoff, J.; Kodambaka, S.; Stach, E. A.; Ross, F. M., Formation of Compositionally Abrupt Axial Heterojunctions in Silicon-Germanium Nanowires. *Science* **2009**, *326* (5957), 1247-1250.
- 6. Gudiksen, M. S.; Lauhon, L. J.; Wang, J.; Smith, D. C.; Lieber, C. M., Growth of nanowire superlattice structures for nanoscale photonics and electronics. *Nature* **2002**, *415* (6872), 617-620.
- 7. Pura, J. L.; Anaya, J.; Souto, J.; Prieto, Á. C.; Rodríguez, A.; Rodríguez, T.; Jiménez, J., Local electric field enhancement at the heterojunction of Si/SiGe axially heterostructured nanowires under laser illumination. *Nanotechnology* **2016**, *27* (45), 455709.

- 8. Kim, S.-K.; Zhang, X.; Hill, D. J.; Song, K.-D.; Park, J.-S.; Park, H.-G.; Cahoon, J. F., Doubling Absorption in Nanowire Solar Cells with Dielectric Shell Optical Antennas. *Nano Letters* **2015**, *15* (1), 753-758.
- 9. Boukai, A. I.; Bunimovich, Y.; Tahir-Kheli, J.; Yu, J.-K.; Goddard III, W. A.; Heath, J. R., Silicon nanowires as efficient thermoelectric materials. *Nature* **2008**, *451* (7175), 168-171.
- 10. Zheng, G.; Patolsky, F.; Cui, Y.; Wang, W. U.; Lieber, C. M., Multiplexed electrical detection of cancer markers with nanowire sensor arrays. *Nature Biotechnology* **2005**, *23* (10), 1294-1301.
- 11. Rotenberg, M. Y.; Elbaz, B.; Nair, V.; Schaumann, E. N.; Yamamoto, N.; Sarma, N.; Matino, L.; Santoro, F.; Tian, B., Silicon Nanowires for Intracellular Optical Interrogation with Subcellular Resolution. *Nano Letters* **2020**, *20* (2), 1226-1232.
- Liu, R.; Chen, R.; Elthakeb, A. T.; Lee, S. H.; Hinckley, S.; Khraiche, M. L.; Scott, J.; Pre, D.; Hwang, Y.; Tanaka, A.; Ro, Y. G.; Matsushita, A. K.; Dai, X.; Soci, C.; Biesmans, S.; James, A.; Nogan, J.; Jungjohann, K. L.; Pete, D. V.; Webb, D. B.; Zou, Y.; Bang, A. G.; Dayeh, S. A., High Density Individually Addressable Nanowire Arrays Record Intracellular Activity from Primary Rodent and Human Stem Cell Derived Neurons. *Nano Letters* **2017**, *17* (5), 2757-2764.
- 13. Periwal, P.; Sibirev, N. V.; Patriarche, G.; Salem, B.; Bassani, F.; Dubrovskii, V. G.; Baron, T., Composition-Dependent Interfacial Abruptness in Au-Catalyzed Si_{1-x}Ge_x/Si/Si_{1-x}Ge_x Nanowire Heterostructures. *Nano Letters* **2014**, *14* (9), 5140-5147.

- 14. Joan, M. R.; Kok-Keong, L.; Timothy, E. B.; Ling, P.; Elizabeth, C. D.; Carim, A. H.; Yanfeng, W.; Marco, A. C.; Theresa, S. M. In *Synthesis and properties of Si and SiGe/Si nanowires*, Proc.SPIE, 2004.
- 15. Periwal, P.; Bassani, F.; Patriarche, G.; Latu-Romain, L.; Brouzet, V.; Salem, B.; Baron, T., Interfacial abruptness in axial Si/SiGe heterostructures in nanowires probed by scanning capacitance microscopy. *Physica Status Solidi A* **2014**, *211* (2), 509-513.
- 16. Fuhrer, A.; Fröberg, L. E.; Pedersen, J. N.; Larsson, M. W.; Wacker, A.; Pistol, M.-E.; Samuelson, L., Few Electron Double Quantum Dots in InAs/InP Nanowire Heterostructures. *Nano Letters* **2007**, *7* (2), 243-246.
- 17. Wu, Y.; Fan, R.; Yang, P., Block-by-Block Growth of Single-Crystalline Si/SiGe Superlattice Nanowires. *Nano Letters* **2002**, *2* (2), 83-86.
- 18. Björk, M. T.; Ohlsson, B. J.; Sass, T.; Persson, A. I.; Thelander, C.; Magnusson, M. H.; Deppert, K.; Wallenberg, L. R.; Samuelson, L., One-dimensional Steeplechase for Electrons Realized. *Nano Letters* **2002**, *2* (2), 87-89.
- 19. Björk, M. T.; Ohlsson, B. J.; Thelander, C.; Persson, A. I.; Deppert, K.; Wallenberg, L. R.; Samuelson, L., Nanowire resonant tunneling diodes. *Applied Physics Letters* **2002**, *81* (23), 4458-4460.
- 20. Hochbaum, A. I.; Fan, R.; He, R.; Yang, P., Controlled Growth of Si Nanowire Arrays for Device Integration. *Nano Letters* **2005**, *5* (3), 457-460.

- 21. Heurlin, M.; Magnusson, M. H.; Lindgren, D.; Ek, M.; Wallenberg, L. R.; Deppert, K.; Samuelson, L., Continuous gas-phase synthesis of nanowires with tunable properties. *Nature* **2012**, *492* (7427), 90-94.
- 22. Metaferia, W.; Persson, A. R.; Mergenthaler, K.; Yang, F. F.; Zhang, W.; Yartsev, A.; Wallenberg, R.; Pistol, M. E.; Deppert, K.; Samuelson, L.; Magnusson, M. H., GaAsP Nanowires Grown by Aerotaxy. *Nano Letters* **2016**, *16* (9), 5701-5707.
- 23. Barrigón, E.; Hultin, O.; Lindgren, D.; Yadegari, F.; Magnusson, M. H.; Samuelson, L.; Johansson, L. I. M.; Björk, M. T., GaAs Nanowire pn-Junctions Produced by Low-Cost and High-Throughput Aerotaxy. *Nano Letters* **2018**, *18* (2), 1088-1092.
- 24. Laocharoensuk, R.; Palaniappan, K.; Smith, N. A.; Dickerson, R. M.; Werder, D. J.; Baldwin, J. K.; Hollingsworth, J. A., Flow-based solution–liquid–solid nanowire synthesis. *Nature Nanotechnology* **2013**, *8* (9), 660-666.
- 25. Lu, X.; de la Mata, M.; Arbiol, J.; Korgel, B. A., Colloidal Silicon–Germanium Nanorod Heterostructures. *Chemistry of Materials* **2017**, *29* (22), 9786-9792.
- 26. Lu, X.; Fanfair, D. D.; Johnston, K. P.; Korgel, B. A., High Yield Solution–Liquid–Solid Synthesis of Germanium Nanowires. *Journal of the American Chemical Society* **2005**, *127* (45), 15718-15719.
- 27. Heitsch, A. T.; Fanfair, D. D.; Tuan, H.-Y.; Korgel, B. A., Solution–Liquid–Solid (SLS) Growth of Silicon Nanowires. *Journal of the American Chemical Society* **2008**, *130* (16), 5436-5437.

- 28. Mujica, M.; Tutuncuoglu, G.; Shetty, P. P.; Mohabir, A. T.; Woods, E. V.; Breedveld, V.; Behrens, S. H.; Filler, M. A., The Geode Process: Hollow Silica Microcapsules as a High Surface Area Substrate for Semiconductor Nanowire Growth. *ACS Applied Nano Materials* **2020**, *3* (1), 905-913.
- 29. Cui, Y.; Lauhon, L. J.; Gudiksen, M. S.; Wang, J.; Lieber, C. M., Diameter-controlled synthesis of single-crystal silicon nanowires. *Applied Physics Letters* **2001**, *78* (15), 2214-2216.
- 30. Shin, N.; Chi, M.; Filler, M. A., Interplay between Defect Propagation and Surface Hydrogen in Silicon Nanowire Kinking Superstructures. *ACS Nano* **2014**, *8* (4), 3829-3835.
- 31. Latu-Romain, L.; Mouchet, C.; Cayron, C.; Rouviere, E.; Simonato, J.-P., Growth parameters and shape specific synthesis of silicon nanowires by the VLS method. *Journal of Nanoparticle Research* **2008**, *10* (8), 1287-1291.
- 32. Pinion, C. W.; Nenon, D. P.; Christesen, J. D.; Cahoon, J. F., Identifying Crystallization-and Incorporation-Limited Regimes during Vapor–Liquid–Solid Growth of Si Nanowires. *ACS Nano* **2014**, *8* (6), 6081-6088.
- 33. Kim, S.; Hill, D. J.; Pinion, C. W.; Christesen, J. D.; McBride, J. R.; Cahoon, J. F., Designing Morphology in Epitaxial Silicon Nanowires: The Role of Gold, Surface Chemistry, and Phosphorus Doping. *ACS Nano* **2017**, *11* (5), 4453-4462.
- 34. Musin, I. R.; Shin, N.; Filler, M. A., Diameter modulation as a route to probe the vapour–liquid–solid growth kinetics of semiconductor nanowires. *Journal of Materials Chemistry C* **2014**, *2* (17), 3285-3291.

- 35. Sivaram, S. V.; Shin, N.; Chou, L.-W.; Filler, M. A., Direct Observation of Transient Surface Species during Ge Nanowire Growth and Their Influence on Growth Stability. *Journal of the American Chemical Society* **2015**, *137* (31), 9861-9869.
- 36. Sivaram, S. V.; Hui, H. Y.; de la Mata, M.; Arbiol, J.; Filler, M. A., Surface Hydrogen Enables Subeutectic Vapor–Liquid–Solid Semiconductor Nanowire Growth. *Nano Letters* **2016**, *16* (11), 6717-6723.
- 37. Christesen, J. D.; Pinion, C. W.; Hill, D. J.; Kim, S.; Cahoon, J. F., Chemically Engraving Semiconductor Nanowires: Using Three-Dimensional Nanoscale Morphology to Encode Functionality from the Bottom Up. *The Journal of Physical Chemistry Letters* **2016**, *7* (4), 685-692.
- 38. Lopez, F. J.; Hemesath, E. R.; Lauhon, L. J., Ordered Stacking Fault Arrays in Silicon Nanowires. *Nano Letters* **2009**, *9* (7), 2774-2779.
- 39. Lopez, F. J.; Givan, U.; Connell, J. G.; Lauhon, L. J., Silicon Nanowire Polytypes: Identification by Raman Spectroscopy, Generation Mechanism, and Misfit Strain in Homostructures. *ACS Nano* **2011**, *5* (11), 8958-8966.
- 40. Adu, K. W.; Gutiérrez, H. R.; Kim, U. J.; Eklund, P. C., Inhomogeneous laser heating and phonon confinement in silicon nanowires: A micro-Raman scattering study. *Physical Review B* **2006**, *73* (15), 155333.
- 41. Lloyd, G. E., Atomic number and crystallographic contrast images with the SEM: a review of backscattered electron techniques. *Mineralogical Magazine* **1987**, *51* (359), 3-19.

- 42. Picraux, S. T.; Dayeh, S. A.; Manandhar, P.; Perea, D. E.; Choi, S. G., Silicon and germanium nanowires: Growth, properties, and integration. *JOM* **2010**, *62* (4), 35-43.
- 43. Peng, W.; Rupich, S. M.; Shafiq, N.; Gartstein, Y. N.; Malko, A. V.; Chabal, Y. J., Silicon Surface Modification and Characterization for Emergent Photovoltaic Applications Based on Energy Transfer. *Chemical Reviews* **2015**, *115* (23), 12764-12796.
- 44. Boles, M. A.; Ling, D.; Hyeon, T.; Talapin, D. V., The surface science of nanocrystals. *Nature Materials* **2016**, *15* (2), 141-153.
- 45. Akin, C.; Yi, J.; Feldman, L. C.; Durand, C.; Hus, S. M.; Li, A.-P.; Filler, M. A.; Shan, J. W., Contactless Determination of Electrical Conductivity of One-Dimensional Nanomaterials by Solution-Based Electro-orientation Spectroscopy. *ACS Nano* **2015**, *9* (5), 5405-5412.
- 46. Akin, C.; Feldman, L. C.; Durand, C.; Hus, S. M.; Li, A.-P.; Hui, H. Y.; Filler, M. A.; Yi, J.; Shan, J. W., High-throughput electrical measurement and microfluidic sorting of semiconductor nanowires. *Lab on a Chip* **2016**, *16* (11), 2126-2134.

TOC Figure

